Supporting Information

SI Materials and Methods

TS Structure. The TS structure was taken from a previously published *ab initio* calculation (1). To assist with defining geometric constraints in the calculations, a pseudoatom (PSA) with no charge and a negligible radius was added 0.01 Å from the acidic proton in the plane of the TS.

Scaffold Selection. For the initial design, the xylanase from the thermophilic fungus *T. aurantiacus* (TAX) was selected as the scaffold. The crystal structure (PDB code: 1GOR) is 1.7 Å resolution with xylobiose bound in the active site (2). The PDB structure was used without minimization, and hydrogens were added with Molprobity (3). Later designs used the native binding pockets of *T. maritima* imidazoleglycerolphosphate synthase (PDB code: 1THF) (4) and *S. solfataricus* indole-3-glycerolphosphate synthase (PDB code: 1A53) (5) as scaffolds.

Gene Synthesis and Cloning. The gene for the wild-type scaffold was back-translated from the protein sequence using the codon usage bias of *Escherichia coli* in DNA 2.0 (6). The DNA sequence for a Factor Xa cleavage site and six-histidine purification tag were added to the 3′ end of the gene. Overlapping oligonucleotides spanning the gene sequence and flanking primers were designed using the Assembly PCR Oligo Maker web server (7). The full-length gene was constructed by recursive PCR using a method based on the one described by Stemmer and coworkers (8). After amplification, the full-length gene was inserted into a pET11a vector (Novagen) using BamHI and NdeI.

Multiple Protein Expression and Purification Protocols. To confirm the activity of HG-3 (HG-2/S265T), independent expression and purification schemes were carried out at two different laboratories. (i) All the designed enzymes and their variants were expressed and purified in the Division of Chemistry and Chemical Engineering, California Institute of Technology, Pasadena, CA using protocol 1. (ii) HG-3 and point mutants were expressed and purified using independent protocols in the Laboratory of Organic Chemistry, ETH Zurich, Zurich, Switzerland using protocol 2. Comparable catalytic activity was observed in both labs.

Protein Expression and Purification: Protocol 1. HG-2, HG-3, 1A53-1, 1A53-2, 1A53-3, 1THF-1, 1THF-2 and all variants were expressed in BL-21 (DE3) *Escherichia coli* cells in LB-Amp. A single colony was used to inoculate overnight cultures of LB-Amp, grown at 37 °C. One liter of LB medium supplemented with 100 mg/L of ampicillin (LB-Amp) was inoculated with 30 mL of the overnight culture. The cells were grown with shaking at 37 °C until OD_{600} ~ 0.3; the temperature was then reduced to 18 °C until OD_{600} ~ 0.6. Protein expression was induced with 1 mM isopropyl β-D-1-thiogalactopyranoside (IPTG) and carried out at 18 °C for 12-18 h. Cells were harvested by centrifugation and resuspended in 30 mL lysis buffer (20 mM Tris pH 7.4, 300 mM NaCl) containing 10 mM imidazole; 10 mM $MgCl_2$, ribonuclease A, and deoxyribonuclease I were added and the cells were lysed mechanically with an Emulsiflex-C5 (Avestin). The soluble fraction was incubated for ~1 h with 1 mL Ni-NTA resin (Qiagen) pre-equilibrated with 10 bed volumes of lysis buffer containing 10 mM imidazole. The resin was washed in a gravity column with 10 bed

volumes of buffer 2 (lysis buffer with 20 mM imidazole) and purified protein was eluted with 3 bed volumes of buffer 3 (lysis buffer with 250 mM imidazole). The eluate was concentrated using Amicon centrifugal concentrators (Millipore) and the buffer was exchanged to 50 mM sodium citrate, 150 mM NaCl pH 5.5 (for 1GOR-based designs) or 25 mM HEPES, 100 mM NaCl pH 7.25 (for 1THF- and 1A53-based designs) using PD-10 desalting columns (GE). Protein purity was confirmed by SDS-PAGE. The molecular weights of all proteins were confirmed by electrospray ionization mass spectrometry. Protein concentrations were determined by measuring the absorbance at 280 nm using the calculated extinction coefficient (ε = 57,410 M^{-1} cm^{-1}).

Protein Expression and Purification: Protocol 2. Here, protein expression was carried out as above except that cultures contained 150 mg/L ampicillin, expression cultures were inoculated with the overnight culture at a ratio of 1:100, and induction was carried out for 24 h. After 24 h, the cells were harvested and resuspended in sonication buffer (20 mM Tris pH 7.4, 300 mM NaCl) containing 10 mM imidazole. Cell lysis was achieved by the addition of 1 mg/mL lysozyme and subsequent sonication. The soluble fraction was applied to Ni-NTA slurry (Qiagen), washed with 20 mM imidazole and then with 32.5 mM imidazole before elution with 250 mM imidazole in sonication buffer. The protein was dialyzed into 20 mM Tris, 20 mM NaCl (pH 8.0) for 16 h and then purified by anion exchange chromatography (MonoQ column, GE Healthcare) in the same buffer, eluting with a salt gradient (20 mM to 1,000 mM NaCl). The protein was concentrated using an Amicon Ultra-15 unit (Millipore).

5-Nitrobenzisoxazole (5-NBZ). This compound was prepared according to literature procedures (9, 10).

CD Spectroscopy. Far-UV spectra were measured at 25 °C using an Aviv 62DS spectropolarimeter equipped with a thermoelectric temperature controller (Aviv Associates, Lakewood, NJ). Thermal denaturations were monitored at 222 nm. All experiments were carried out in a 1 mM cuvette containing 10 μM protein in 25 mM HEPES pH 7.25, 100 nM NaCl. Apparent midpoints of thermal denaturation (T_m) were obtained using the equation of Minor and Kim (11). T_m values should be considered approximate and not actual thermodynamic parameters, as the denaturation was not reversible in any case tested.

Mass Spectrometry. The protein sample was desalted using a C_4 ZipTip (Millipore) and measured in 50% acetonitrile/0.2% formic acid (pH 2.0) by electrospray ionization mass spectrometry (ESI-MS) on a Q-TOF Ultima mass spectrometer (Waters). The mass spectrum of each protein was deconvoluted using MaxEnt1 software.

Protein Crystallization and Crystallography. Crystals of HG-1 (expressed and purified using protocol 1) were obtained at room temperature from a 4 mL hanging drop containing 5 mg/mL HG-1 in buffer containing 0.8 M potassium-sodium tartrate, 0.1 M Tris pH 8.5, 0.5% PEG-MME 5000. The crystal was cryo-protected in the reservoir solution with 15% ethylene glycol. Data were collected using a MicroMax-007HF X-ray generator with a RAXIS IV++ detector (Rigaku Corp.) All data were processed using CrystalClear (Rigaku Corp.) and MOSFLM (12).

Crystals of HG-2/NBT, 1A53-2/NBT, and apo 1A53-2 were obtained through sitting-drop vapor diffusion carried out at room temperature with a protein concentration of 9.5 mg/mL. Co-crystallization for HG-2/NBT and 1A53-2/NBT was achieved through pre-incubation of the protein with 5 mM 5-nitrobenzotriazole (5-NBT, Ryan Scientific) prior to crystallization trials. A 100 mM stock solution of 5-NBT was prepared in DMSO before combining with the protein. Reservoir solutions for HG-2/NBT (0.1 M sodium acetate pH 4.6, 2 M ammonium sulfate), 1A53-2/NBT (0.1 M sodium citrate/citric acid pH 5.6, 0.2 M potassium sodium tartrate, 2 M ammonium sulfate), and apo 1A53-2 (0.1 M Bis-Tris pH 5.5, 0.2 M ammonium acetate, and 25% PEG 3350) were combined with protein in a 1:1 ratio. A single HG-2/NBT, multiple cube-like 1A53-2/NBT, and several plate-like apo 1A53-2 crystals developed with a minimum growth time of one month. The crystals were cryo-protected with paraffin oil and shipped to the Stanford Synchrotron Radiation Lightsource, beamline 12-2 for remote data collection. Diffraction data were processed with the program MOSFLM using the interface iMOSFLM (12).

Data were scaled using the program SCALA (13). Molecular replacement was carried out with PHASER (13, 14). The coordinates for *Thermoascus aurantiacus* xylanase I (PDB code: 1GOR) (2) and *Sulfolobus solfataricus* (PDB code: 1A53) (5) were modified to contain alanine at all point mutations in the designs and were subsequently used as the molecular replacement starting models for HG-2 and 1A53-2, respectively. Model building was carried out using COOT (15). The structure was refined using REFMAC (16) and PHENIX (17). Backbone density for the HG-2 structure appeared in two distinct backbone conformations in chain B, similar to the dual backbone conformation found in the structure of red fluorescent protein variant FP611 (PDB code: 3E5T) (18). The apo structure of 1A53-2 was processed with a twinning fraction of 0.13 towards the end of refinement. Crystallographic data statistics are summarized in Table S2.

Kinetic Measurements. Assays were carried out with 5 μM protein (purified via protocol 1) in 25 mM HEPES, pH 7.25, 100 mM NaCl at 27 °C. Substrate concentrations between 16 μM and 1 mM were used and the acetonitrile concentration was kept constant at 2% of the 1 mL reaction volume. Product formation was monitored at 380 nm (ε = 15,800 $cm^{-1}M^{-1}$) using a Shimadzu UV-1601 spectrophotometer. Initial reaction rates were determined from the linear portion of the reaction progress curve and were corrected for the initial rate contribution for the buffer catalyzed (no protein) reaction. Kaleidagraph (Synergy Software) was used to fit the data to the Michaelis-Menten equation to determine the kinetic parameters k_{cat} and K_m:

$$\frac{v_0}{[E]_T} = \frac{k_{cat} \cdot [S]_0}{K_m + [S]_0}$$

where v_0 is the initial reaction rate, $[E]_T$ is the total enzyme concentration, and $[S]_0$ is the initial substrate concentration. In the cases where the enzyme was not saturated because of limited substrate solubility, the data were fit to a line to determine k_{cat}/K_m.

Where indicated in Table 1, assays were carried out using 1 μM of protein purified via expression protocol 2 in 50 mM phosphate buffer (pH 7.0), containing 100 mM NaCl and 2% acetonitrile. Reactions were initiated by adding different amounts of 5-NBZ in acetonitrile (25 μM to 1.25 mM final concentration). Product formation was monitored at 380 nm in a Lambda 35 UV/Vis spectrometer (PerkinElmer) at 27 °C.

pH-Rate Profile. For the pH-rate profile, reactions were initiated by addition of 5-NBZ (50 μM final concentration) to 1 to 4 μM protein in the following reaction buffers: 50 mM buffer salt [sodium acetate (pH < 6.0), sodium phosphate (6.0 < pH < 8.0), and sodium carbonate (pH > 8.0)], containing 100 mM NaCl and 2% acetonitrile. Product formation was monitored as described above. The pH of all reaction solutions was confirmed after completion of the reaction using a pH-Meter 526 (Wissenschaftlich-Technische Werkstätten). The data were fit to the equation:

$$k_{cat}/K_m = \frac{(k_{cat}/K_m)^{\max}}{1+10^{pka1-pH}+10^{pH-pKa2}}$$

***K_i* Determination.** After preincubation of 1 μM HG-3 with varying concentrations of 5-nitrobenzotriazole (0.001–1000 μM final concentrations) in 50 mM acetate buffer (pH 5) containing 100 mM NaCl, 2% acetonitrile, and 1% DMSO, the reactions were initiated by addition of 5-NBZ (250 μM final concentration). Product formation was monitored as described above. The IC_{50} value was determined by curve fitting (Hill-Slope model, v_i at infinite inhibitor concentration was set to zero) and subsequently converted into the corresponding K_i value using the Cheng-Prusoff equation $K_i = [IC_{50}]/(1+[S]/K_m)$ (19). The K_m value was determined independently in the same buffer and under identical reaction conditions using the protocol described above.

MD Simulations. MD simulations were carried out for 20 ns for each enzyme-substrate complex at NPT conditions (constant number of particles, pressure, and temperature) with a pressure of 1 bar and temperature of 300 K. The TIP3P explicit solvent model (20) was used to solvate the protein in an octahedral-shaped volume, ensuring a solvent layer of at least 10 Å from any point on the protein surface. Each face of the octahedral box is connected to a mirror image of itself, which allows the system to be treated with periodic boundary conditions. This ensures equilibration through diffusion while the number of particles is kept constant. The temperature is regulated and evenly distributed through a Langevin equilibration scheme. The 5-NBZ substrate was parameterized from quantum mechanical calculations in order to be treated correctly by the AMBER force field (21). Prior to production MD, the substrate was superimposed onto the ab initio transition state in the active site of the computationally designed protein model. The structure of the resulting protein-substrate complex was optimized and heated to 300 K in six 50 ps steps for a total of 300 ps at NVT conditions, and then equilibrated at NPT conditions for 2 ns.

The structural models predicted by the computational design algorithm were used as starting structures. Substrate parameters were generated within the Antechamber module of AMBER 10 (22) using the general AMBER force field, with partial charges set to fit the electrostatic potential generated at HF/6-31G* by RESP (23). The charges were calculated according to the Merz-Singh-Kollman scheme (24, 25) using Gaussian 03 (26).

The structures were immersed in a truncated octahedral box with a 10 Å buffer of TIP3P (20) water molecules, resulting in the addition of up to 16,000 solvent molecules, depending on the scaffold. The systems were neutralized by addition of explicit counter ions. All subsequent calculations were done using the widely tested Stony Brook modification of the AMBER 99 force field (27). A two-stage geometry optimization approach was utilized, initially minimizing the positions of water molecules and ions, followed by an unrestrained minimization of all atoms. The systems were heated gently in six steps of 50 ps from 0 to 300 K at constant volume periodic boundary conditions. Weak

harmonic restraints of 30 kcal/mol were applied to the solute, and the Langevin equilibration scheme was used to control and equalize the temperature. The time step was kept at 1 fs during the heating stages, allowing potential inhomogeneities to self-adjust. Each system was then equilibrated for 2 ns with a 2 fs time step at a constant pressure of 1 atm. Water molecules were triangulated with the SHAKE algorithm such that the angle between the hydrogen atoms is kept fixed. A 20 ns production MD simulation was performed for each of the systems (with and without the substrate bound to the active site) using PMEMD (28). Geometries and velocities were saved every 100 steps (0.2 ps), which resulted in a total of 10,000 and 100,000 frames from each production run. Long-range electrostatic effects were modeled using the particle-mesh-Ewald method (29). Post-MD data extraction and analysis were performed using the ptraj module of AMBER 10 (22) and the statistical analysis software OriginPro8 (Origin Lab).

QM Calculations. Theozyme DFT B3LYP/6-31G(d) transition state (TS) calculations were performed on a model system that consists of the substrate, acetate as the general base, and methanol as the hydrogen-bond donor. The distance versus angle scatter-point of the deprotonation is plotted in Figure 3C and 3D.

Table S1. Geometric constraints for the contact between the TS and the catalytic residues

Contact: Asp/Glu to H3*

Residue	Type	Atom1	Atom2	Atom3	Atom4	Min[†,‡]	Max[†,‡]
Asp	Distance	OD1	H3			1.0	1.6
	Angle	OD2	OD1	H3		59.0	121.0
	Torsion	CG	OD2	OD1	H3	159.0	201.0
	Angle	OD1	H3	PSA		59.0	121.0
	Torsion	OD2	OD1	H3	PSA	0.0	360.0
	Torsion	OD1	H3	PSA	C3	159.0	201.0
Asp	Distance	OD2	H3			1.0	1.6
	Angle	OD1	OD2	H3		59.0	121.0
	Torsion	CG	OD1	OD2	H3	159.0	201.0
	Angle	OD2	H3	PSA		59.0	121.0
	Torsion	OD1	OD2	H3	PSA	0.0	360.0
	Torsion	OD2	H3	PSA	C3	159.0	201.0
Glu	Distance	OE1	H3			1.0	1.6
	Angle	OE2	OE1	H3		59.0	121.0
	Torsion	CD	OE2	OE1	H3	159.0	201.0
	Angle	OE1	H3	PSA		59.0	121.0
	Torsion	OE2	OE1	H3	PSA	0.0	360.0
	Torsion	OE1	H3	PSA	C3	159.0	201.0
Glu	Distance	OE2	H3			1.0	1.6
	Angle	OE1	OE2	H3		59.0	121.0
	Torsion	CD	OE1	OE2	H3	159.0	201.0
	Angle	OE2	H3	PSA		59.0	121.0
	Torsion	OE1	OE2	H3	PSA	0.0	360.0
	Torsion	OE2	H3	PSA	C3	159.0	201.0

Contact: Ser/Thr/Tyr to O1*

Residue	Type	Atom1	Atom2	Atom3	Atom4	Min[†,‡]	Max[†,‡]
Ser	Distance	OG	O1			2.6	4.0
	Angle	OG	HG	O1		150.0	180.0
	Angle	HG	O1	N2		100.0	160.0
	Torsion	HG	O2	N2	C3	120.0	240.0
Thr	Distance	OG1	O1			2.6	4.0
	Angle	OG1	HG1	O1		150.0	180.0
	Angle	HG1	O1	N2		100.0	160.0
	Torsion	HG1	O2	N2	C3	120.0	240.0
Tyr	Distance	OH	O1			2.6	4.0
	Angle	OH	HH	O1		150.0	180.0
	Angle	HH	O1	N2		100.0	160.0
	Torsion	HH	O2	N2	C3	120.0	240.0

*Three contacts were required: Asp/Glu, Phe/Trp, and Ser/Thr/Tyr.
[†]Distance measurements are given in Å.
[‡]Angle, torsion, and plane measurements are given in degrees.

Contact: Phe/Trp to PS2*

Residue	Type	Atom1	Atom2	Atom3	Atom4	Atom5	Atom6	Min[†,‡]	Max[†,‡]
Phe	Pseudo-atom	PS1, equidistant between CE1 and CD2							
	Pseudo-atom	PS2, equidistant between C4 and C9							
	Distance	PS1	PS2					3.0	4.0
	Plane	CG	CE1	CE2	C5	C8	N2	0.0	40.0
Trp	Pseudo-atom	PS1, equidistant between CE2 and CD2							
	Pseudo-atom	PS2, equidistant between C4 and C9							
	Distance	PS1	PS2					3.0	4.0
	Plane	CD1	CE3	CH2	C5	C8	N2	0.0	40.0

*Three contacts were required: Asp/Glu, Phe/Trp, and Ser/Thr/Tyr.
[†]Distance measurements are given in Å.
[‡]Angle, torsion, and plane measurements are given in degrees.

Table S2. Summary of design calculations for Kemp elimination enzymes

		Allowed residues for required contacts (actual contact)				Active site repacking positions		
Design	Scaffold	Base	π-stacking	H-bond	Active site search design positions[a]	Design*	Float†	Mutations
HG-1	1GOR	E/D (E237)	F/W (W275)	S/T/Y (Y90)	46, 50, 83, 84, 87, 90, 130, 172, 207, 209, 267, 275	21, 46, 83, 87, 89, 239, 267	47, 50, 83, 84, 90, 130, 131, 172, 207, 209, 237, 239, 267, 275, 282	A21M, E46M, W87G, S89F, Q90Y, D239N, W267A
HG-2	1GOR	D (D127)	F/W (T44W)	S/T/Y (T265S)	17, 42, 44, 81, 83, 129, 170, 172, 209, 234, 236, 237, 265, 267	21, 42, 81, 83, 84, 125, 130, 172, 234, 236, 237, 267	16, 17, 46, 47, 50, 79, 87, 90, 170, 207, 209, 239, 275 276	Q42M, T44W, R81G, H83G, T84M, N130G, N172M, A234S, T236L, E237M, T265S, W267F
1THF-1	1THF	E (S101E)	F/W (L50W)	K (L222K)	7, 9, 11, 48, 50, 101, 126, 128, 130, 169, 171, 176, 199, 201, 222, 224	9, 48, 78, 101, 103, 126, 128, 130, 169, 171, 199, 201	7, 11, 176	C9G, V48G, L50W, T78S, S101E, N103M, A128W, D130A, L169A, T171V, I199G, S201M, L222K
1THF-2	1THF	E (S101E)	F/W (L50W/A128W)	S/T/Y (S201)	"	9, 48, 78, 126, 128, 130, 169, 171, 222	7, 11, 176, 199, 224	C9G, V48G, L50W, T78S, S101E, A128W, D130A, L169A, T171L, L222V
1A53-1	1A53	E (L231E)	F/W (K110W)	S/T/Y (L131S)	51, 81, 83, 89, 108, 110, 112, 131, 133, 157, 159, 178, 180, 182, 184, 210, 211, 231	51, 81, 108, 157, 159, 180, 210	83, 89, 112, 133, 178, 182, 184, 211	E51I, S81G, K110W, L131S, L157G, E159W, N180G, E210S, L231E
1A53-2	1A53	E (G178E)	F/W (K110W/E210W)	none	"	51, 81, 83, 108, 131, 157, 159, 180, 211, 231	8, 53, 89, 108, 112, 133, 182, 184	E51A, S81A, L83A, K110W, L131A, K157A, E159V, G178E, N180A, E210E, S211Q, L231G
1A53-3	1A53	E (L157E)	F/W (K110W/E210W)	none	"	81, 83, 108, 131, 178, 180, 211, 231	8, 53, 89, 112, 129, 133, 182, 184	E51L, S81A, L83A, K110W, L131A, L157E, E159I, N180M, E210W, S211Q, L231G

* The positions allowed to change identity during the active site search and repacking calculations are indicated as design residues.
† The positions allowed to change conformation but not identity during the repacking calculation are indicated as float residues.

Table S3. Data collection and refinement statistics for HG-1, HG-2, and 1A53-2 crystal structures

	HG-1 (PDB: 3O2L)	HG-2/NBT (PDB: 3NYD)	1A53-2/NBT (PDB: 3NZ1)	1A53-2 (PDB: 3NYZ)
Data Collection				
Space group	$P2_12_12_1$	$P2_12_12_1$	$P3_121$	$P2_1$
Cell dimensions				
a, b, c, Å	48.3, 72.5, 74.6	75.8, 78.1, 98.2	60.7, 60.7, 120.2	38.0, 46.3, 127.0
α, β, γ, °	90.0, 90.0, 90.0	90.0, 90.0, 90.0	90.0, 90.0, 120.0	90.0, 92.0, 90.0
Resolution, Å	2.0	1.2	1.6	1.5
R_{sym} , %*	2.5 (4.4)	4.6 (33.8)	6.6 (50.4)	11.6 (45.6)
$I/\sigma I$*	30.7 (21.1)	10.3 (1.9)	8.8 (17.6)	4.8 (2.0)
Completeness, %*	99.2 (98.2)	98.8 (96.4)	99.8 (95.8)	99.4 (99.9)
Redundancy*	2.7 (2.6)	3.5 (2.3)	4.0 (3.7)	2.9 (2.9)
Wavelength, Å	1.54	0.99	1.01	1.01
Refinement				
Resolution (Å)*	35.4-2.0 (2.1-2.0)	34.1-1.23 (1.3-1.23)	52.6-1.6 (1.6-1.5)	36.7-1.5 (1.6-1.5)
Number of reflections				
Working set	17130	158059	37189	67105
Test set	874	8337	1856	2041
R_{work}/R_{free} ,%	16.7/22.9	15.7/19.6	17.2/21.0	20.2/25.1
Number of atoms				
Protein	2326	4591	2007	4089
Ligand/Ion	0	50	72	5
Water	218	670	181	237
RMS deviations				
Bond lengths, Å	0.024	0.028	0.027	0.010
Bond angles, °	1.80	2.35	2.40	1.24
Twin fraction	N/A	N/A	N/A	0.13

*Parentheses indicate statistics for outer shell of data.
N/A, not applicable.

Table S4. Variation of contact geometry for targeted ligand placement

Placement: H3 from Aspartate (OD1)

Type	Atom1	Atom2	Atom3	Atom4	Min*,†	Max*,†	Step*,†
Distance	OD1	H3			1.1	1.5	0.2
Angle	OD2	OD1	H3		70.0	110.0	20.0
Torsion	CG	OD2	OD1	H3	160.0	200.0	20.0
Angle	OD1	H3	PSA		70.0	110.0	20.0
Torsion	OD2	OD1	H3	PSA	0.0	360.0	20.0
Torsion	OD1	H3	PSA	C3	160.0	200.0	20.0

Placement: H3 from Aspartate (OD2)

Type	Atom1	Atom2	Atom3	Atom4	Min	Max	Step
Distance	OD2	H3			1.1	1.5	0.2
Angle	OD1	OD2	H3		70.0	110.0	20.0
Torsion	CG	OD1	OD2	H3	160.0	200.0	20.0
Angle	OD2	H3	PSA		70.0	110.0	20.0
Torsion	OD1	OD2	H3	PSA	0.0	360.0	20.0
Torsion	OD2	H3	PSA	C3	160.0	200.0	20.0

Placement: H3 from Glutamate (OE1)

Type	Atom1	Atom2	Atom3	Atom4	Min	Max	Step
Distance	OE1	H3			1.1	1.5	0.2
Angle	OE2	OE1	H3		70.0	110.0	20.0
Torsion	CD	OE2	OE1	H3	160.0	200.0	20.0
Angle	OE1	H3	PSA		70.0	110.0	20.0
Torsion	OE2	OE1	H3	PSA	0.0	360.0	20.0
Torsion	OE1	H3	PSA	C3	160.0	200.0	20.0

Placement: H3 from Glutamate (OE2)

Type	Atom1	Atom2	Atom3	Atom4	Min	Max	Step
Distance	OE2	H3			1.1	1.5	0.2
Angle	OE1	OE2	H3		70.0	110.0	20.0
Torsion	CD	OE1	OE2	H3	160.0	200.0	20.0
Angle	OE2	H3	PSA		70.0	110.0	20.0
Torsion	OE1	OE2	H3	PSA	0.0	360.0	20.0
Torsion	OE2	H3	PSA	C3	160.0	200.0	20.0

The TS was placed at every indicated geometry for every rotamer of Asp or Glu in the active site search calculation.

*Distance measurements are given in Å.

†Angle and torsion measurements are given in degrees.

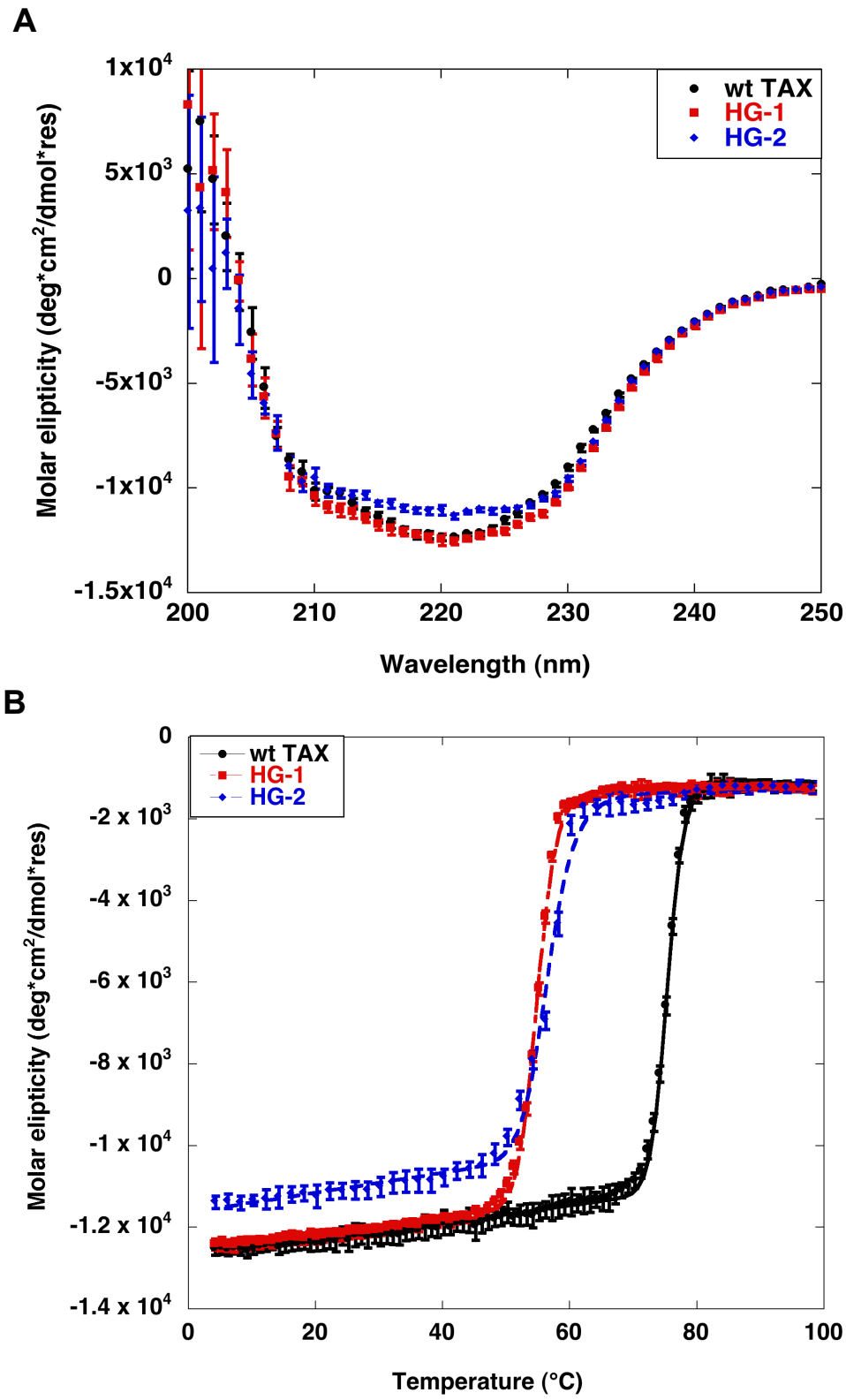

Fig. S1. CD Characterization of HG-1 and HG-2. (A) Far UV wavelength scan. (B) Thermal denaturation.

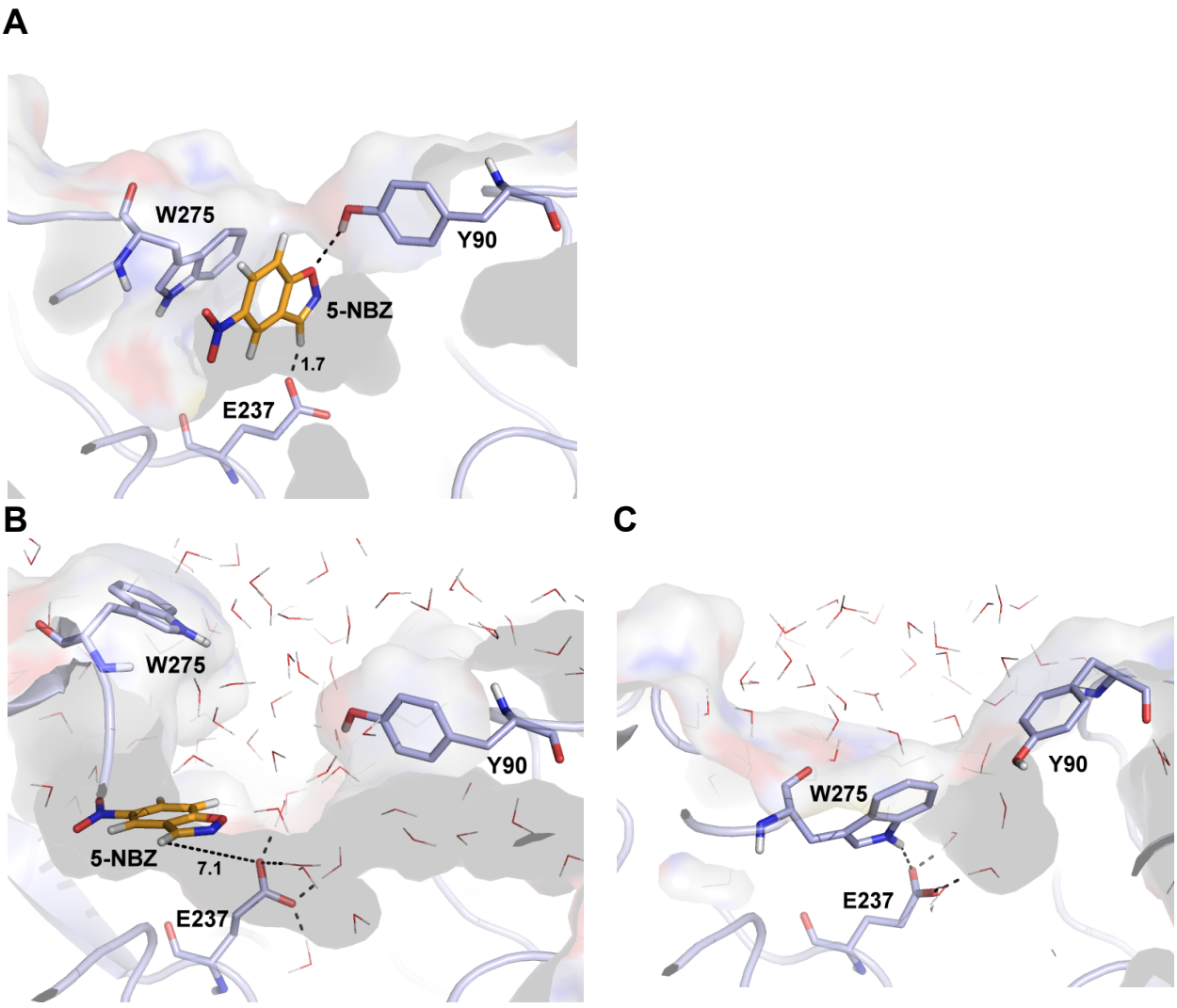

Fig. S2. The active site of HG-1 (*A*) prior to MD, (*B*) after MD on the 5-NBZ:HG-1 complex, and (*C*) after MD in the absence of 5-NBZ. All distance values are in Å.

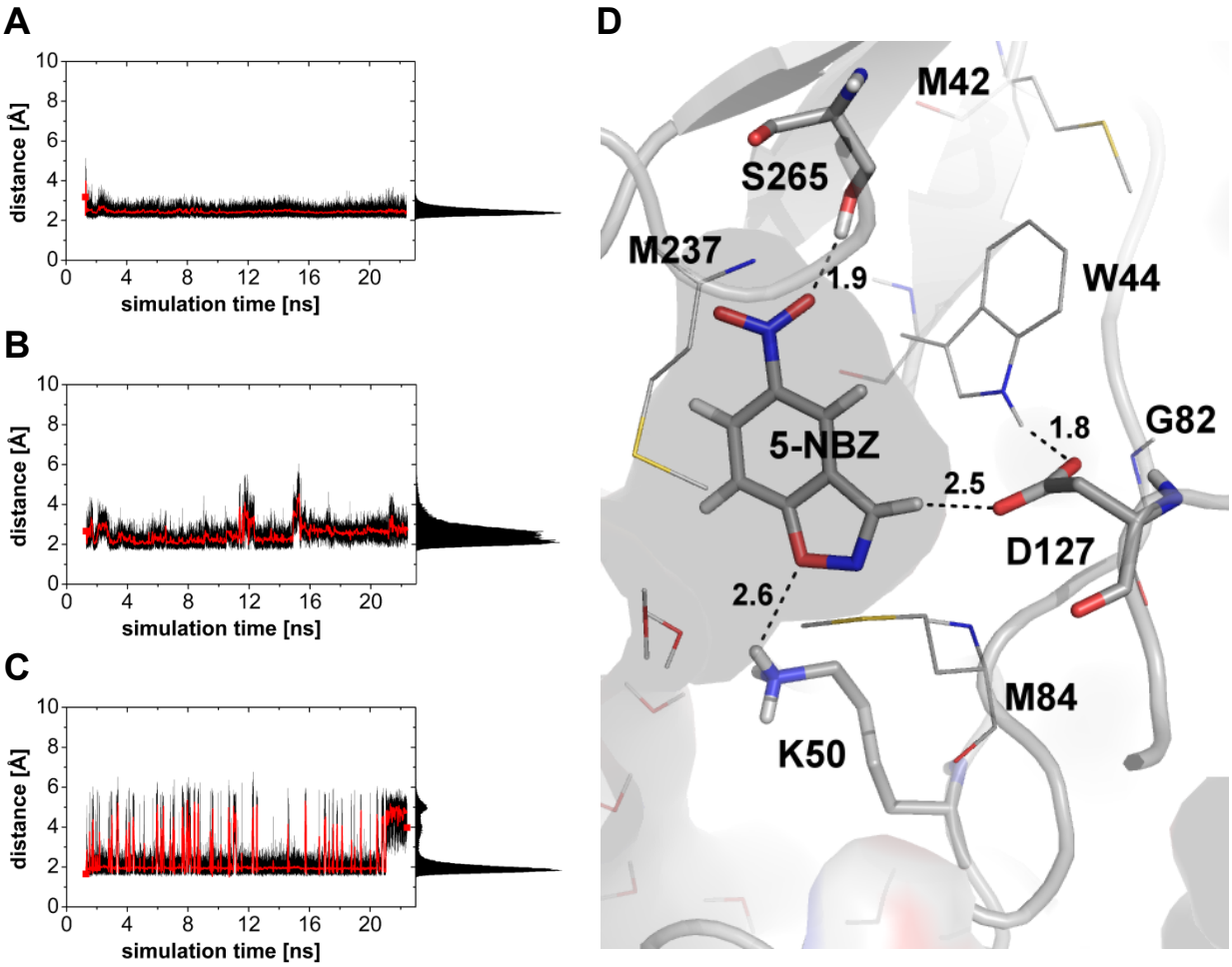

Fig. S3. MD of HG-2 with 5-NBZ bound in an alternative orientation (O2). Distance-time plots and projected distance distributions for the contacts between (*A*) the acidic H of 5-NBZ and the Asp127 carboxylate oxgens, (*B*) the heterocycle oxygen of 5-NBZ and the Hs of Lys50, and (*C*) the nitro group oxygens of 5-NBZ and the OH of Ser265. (*D*) A representative MD snapshot of the HG-2 active site with 5-NBZ bound in orientation O2. All distance values are in Å.

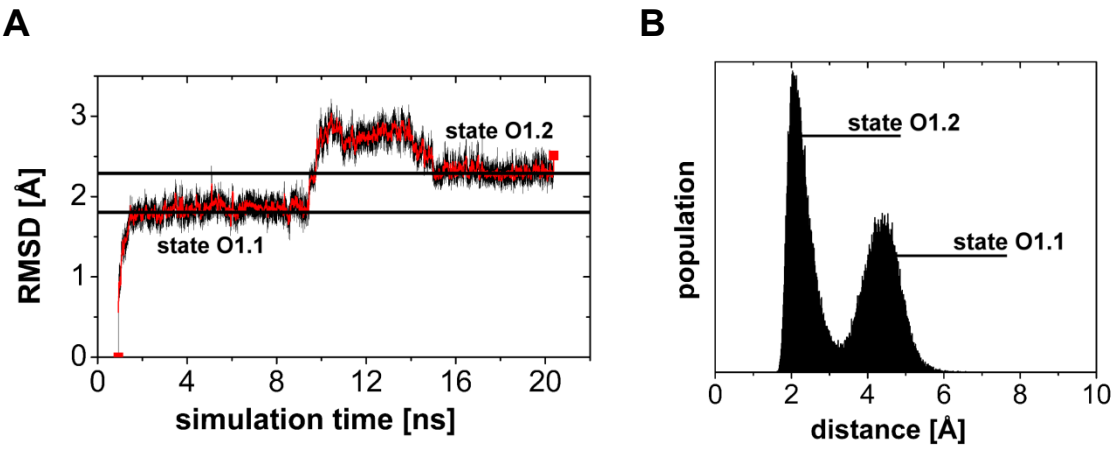

Fig. S4. (*A*) RMSD plot of the active site residues of HG-2. (*B*) Histogram of distance distribution between the carboxylate oxygens of D127 and the backbone NH of G82.

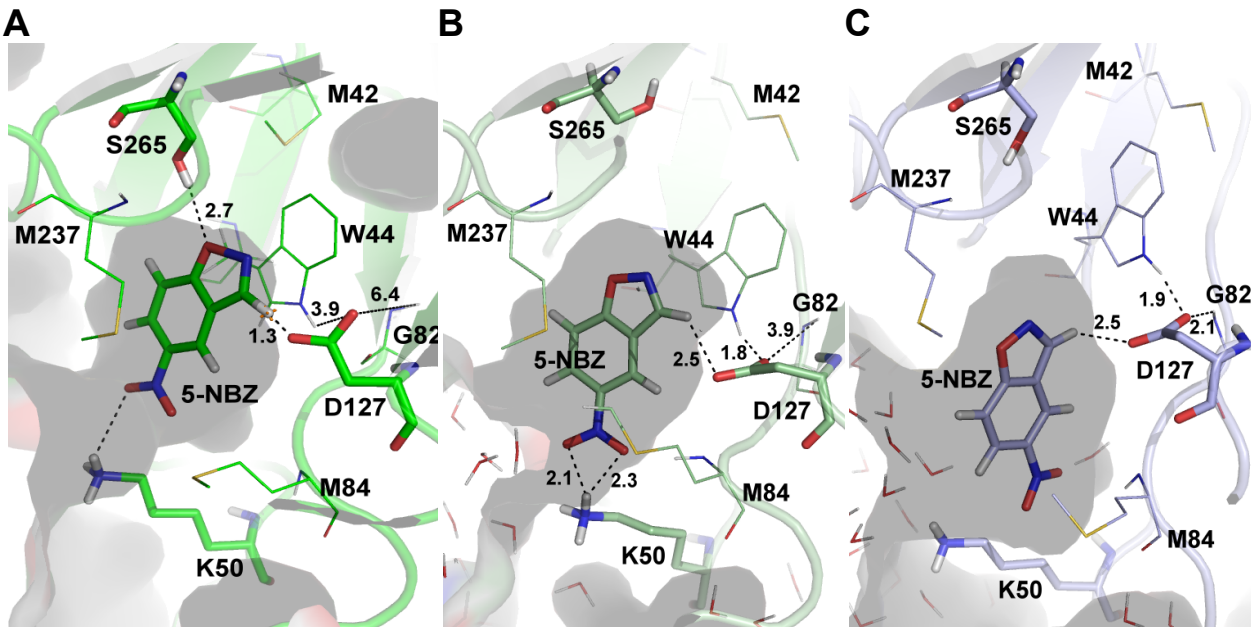

Fig. S5. Active site of HG-2. **(***A***)** Computational design model. **(***B***)** MD snapshot of state 1**.** (*C*) MD snapshot of state 2.

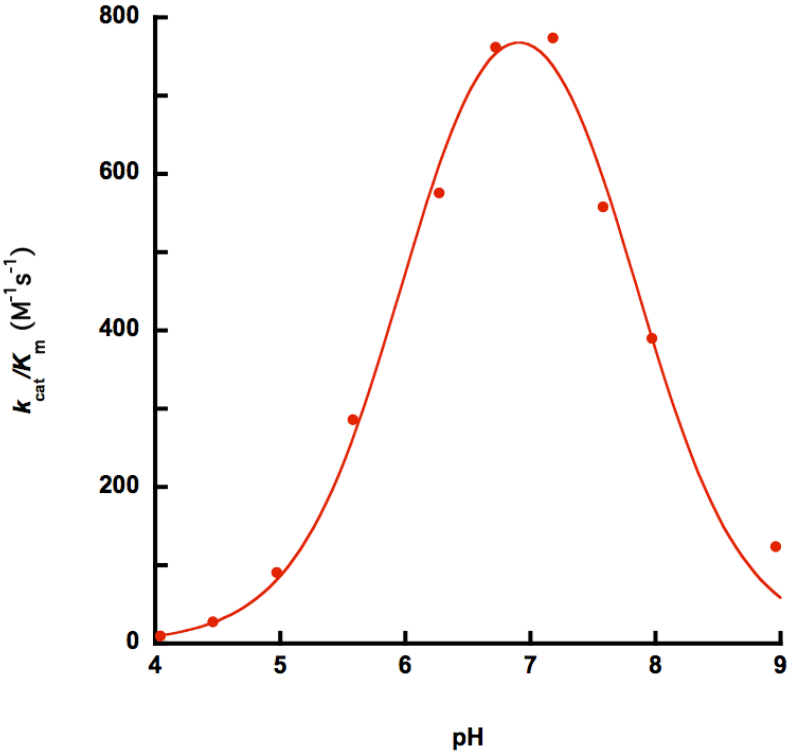

Fig. S6. pH rate profile of HG-2/S265T. HG-2/S265T exhibits a bell-shaped pH-rate profile with inflection points at pH 6.0 and 7.8. The pH optimum of enzymatic activity is at pH 7.0. Experiments were performed in 50 mM acetate (pH 4.0-5.6), phosphate (pH 6.3-8.0), and carbonate (pH 9) buffer, each containing 100 mM NaCl.

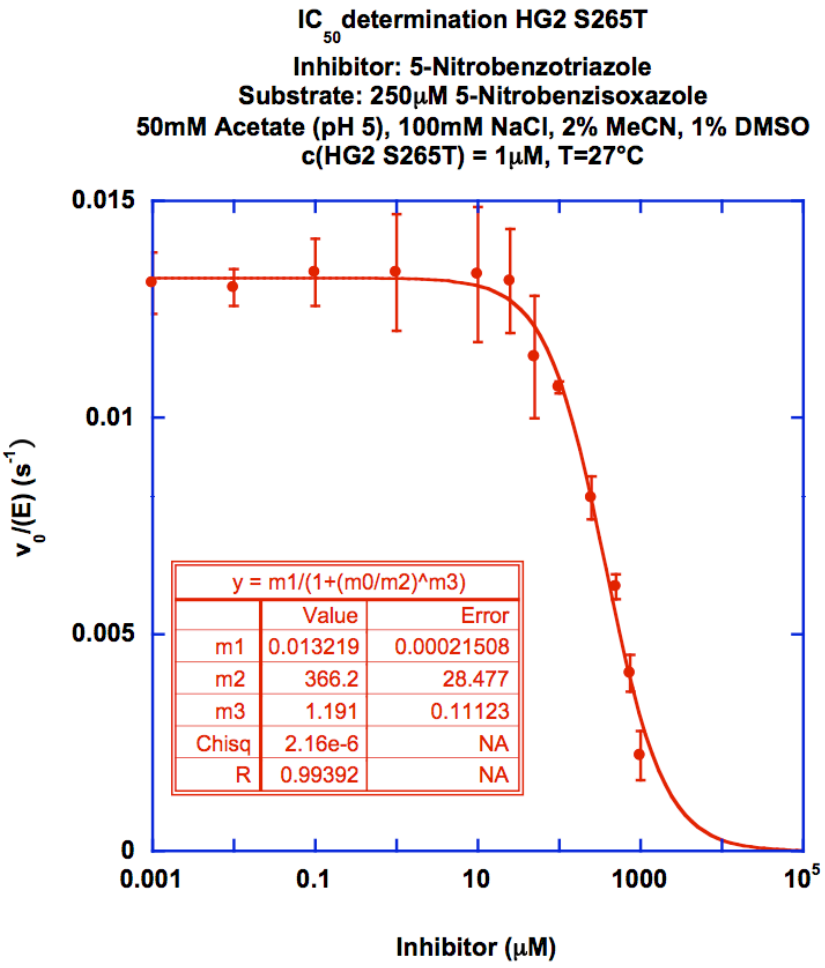

Fig. S7. IC_{50} determination for 5-nitrobenzotriazole and HG-3. The assays were carried out with 250 μM 5-NBZ, 50 mM acetate pH 5.0, 100 mM NaCl, 2% acetonitrile, 1% DMSO, 1 μM enzyme, at 27 °C. In the curve-fit legend, m1 is the difference between $(v_0/E)_{min}$ and $(v_0/E)_{max}$, *m2* is the IC_{50}, and *m3* is the Hill coefficient. In the absence of inhibitor, (HG-3) has an apparent k_{cat} = 0.110 ± 0.006 s^{-1} and K_m = 2.14 ± 0.2 mM under these assay conditions.

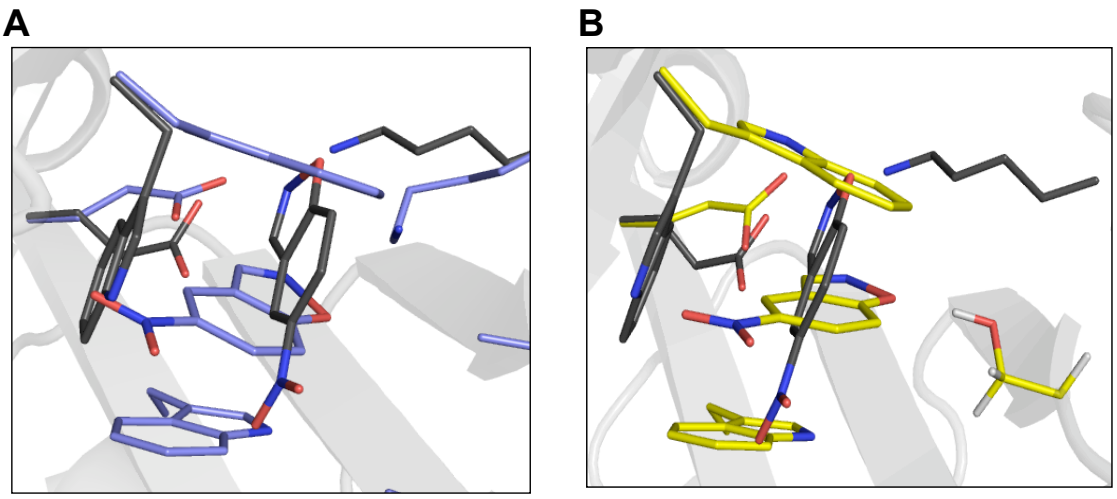

Fig. S8. Overlay of 1THF-based KE design models with KE07 design model (30). (*A*) 1THF-1 catalytic residues (purple sticks) are overlaid with KE07 catalytic residues (grey sticks). (*B*) 1THF-2 catalytic residues (yellow sticks) are overlaid with KE07 catalytic residues (grey sticks).

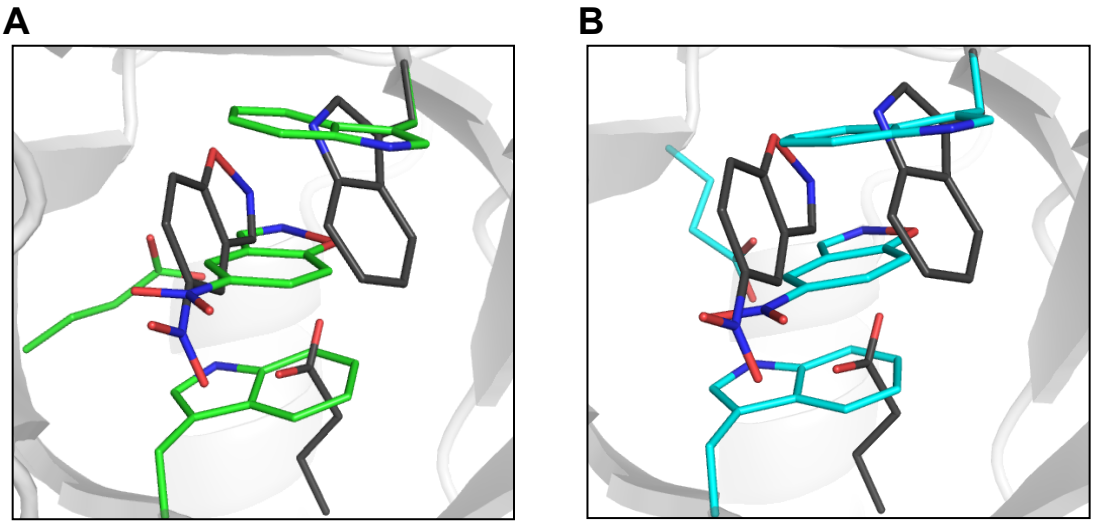

Fig. S9. Overlay of 1A53-based KE design models with KE59 design model (30). (*A*) 1A53-2 catalytic residues (green sticks) are overlaid with KE59 catalytic residues (grey sticks). (*B*) 1A53- catalytic residues (cyan sticks) are overlaid with KE59 catalytic residues (grey sticks).

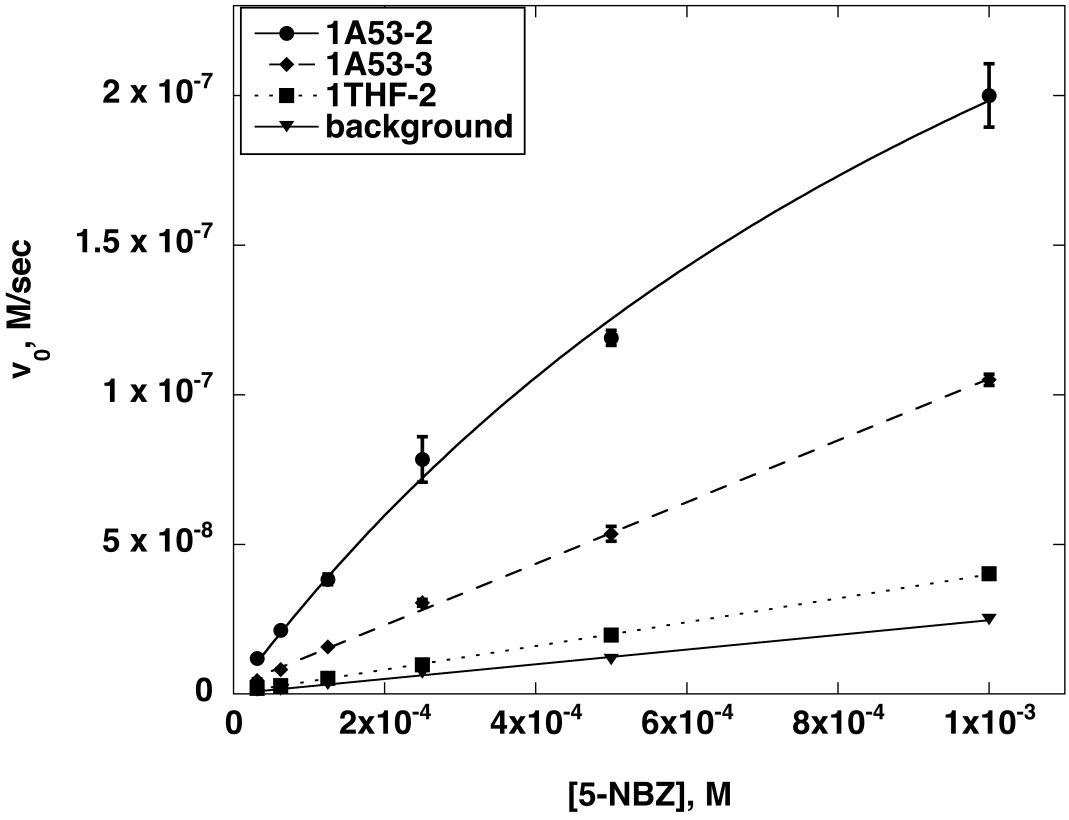

Fig. S10. Michaelis-Menten plots of designed enzymes based on the scaffolds 1A53 and 1THF. Standard errors are calculated from three measurements.

SI References

1. Na J, Houk KN, Hilvert D (1996) Transition state of the base-promoted ring-opening of isoxazoles. Theoretical prediction of catalytic functionalities and design of haptens for antibody production. *J Am Chem Soc* 118:6462-6471.

2. Lo Leggio L, et al. (2001) Substrate specificity and subsite mobility in T. aurantiacus xylanase 10A. *FEBS Letters* 509:303-308.

3. Davis IW, Murray LW, Richardson JS, Richardson DC (2007) MolProbity: all-atom contacts and structure validation for proteins and nucleic acids. *Nucleic Acids Res* 35:W375-W383.

4. Lang D, Thoma R, Henn-Sax M, Sterner R, Wilmanns M (2000) Structural evidence for evolution of the β/α barrel scaffold by gene duplication and fusion. *Science* 289:1546-1550.

5. Hennig M, Darimont BD, Jansonius JN, Kirschner K (2002) The catalytic mechanism of indole-3-glycoerol phosphate synthase: crystal structures of complexes of the

enzyme from Sulfolobus solfataricus with substrate analogue, substrate, and product. *J Mol Biol* 319:757-766.

6. Villalobos A, Ness JE, Gustafsson C, Minshull J, Govindarajan S (2006) Gene Designer: a synthetic biology tool for constructing artificial DNA segments. *BMC Bioinformatics* 7:285-292.

7. Rydzanicz R, Zhao XS, Johnson PE (2005) Assembly PCR oligo maker: a tool for designing oligodeoxynucleotides for constructing long DNA molecules for RNA production. *Nucleic Acids Res* 33:W521-525.

8. Stemmer WP, Crameri A, Ha KD, Brennan TM, Heyneker HL (1995) Single-step assembly of a gene and entire plasmid from large numbers of oligodeoxyribonucleotides. *Gene* 164:49-53.

9. Kemp DS, Woodward RB (1965) The N-ethylbenzisoxazolium cation - I: Preparation and reactions with nucleophilic species. *Tetrahedron* 21:3019-3035.

10. Casey ML, Kemp DS, Paul KG, Cox DD (1973) Physical organic chemistry of benzisoxazoles. I. Mechanism of the base-catalyzed decomposition of benzisoxazoles. *Journal of Organic Chemistry* 38:2294-2301.

11. Minor DL, Kim PS (1994) Measurement of the bold beta-sheet-forming propensities of amino acids. *Nature* 367:660-663.

12. Leslie AGW (1992) Recent changes to the MOSFLM package for processing film and image plate data. *Joint CCP4 + ESF-EAMCB Newsletter on Prot Crystallography* 26

13. Storoni LC, McCoy AJ, Read RJ (2004) Likelihood-enhanced fast rotation functions. . *Acta Crystallographica Section D: Biological Crystallography* 60:432-438.

14. McCoy AJ, Grosse-Kunstleve RW, Storoni LC, Read RJ (2005) Likelihood-enhanced fast translation functions. *Acta Crystallographica Section D* 61:458-464.

15. Emsley P, Cowtan K (2004) Coot: model-building toos for molecular graphics. *Acta Crystallographica Section D* 61:458-464.

16. Murshudov GN, Vagin AA, Dodson EJ (1997) Refinement of macromolecular structures by the maximum-likelihood method. *Acta Crystallographica Section D* 53:240-255.

17. Adams PD, et al. (2002) PHENIX: building new software for automated crystallographic structure determination. *Acta Crystallographica Section D: Biological Crystallography* 58:1948-1954.

18. Nienhaus K, Nar H, Heilker R, Wiedenmann J, Nienhaus GU (2008) Trans-cis isomerization is responsible for the red-shifted fluorescence in variants of the red fluorescent protein eqFP611. *J Am Chem Soc* 130:12578-12579.

19. Cheng Y, Prusoff WH (1973) Relationship between the inhibition constant (K1) and the concentration of Inhibitor which causes 50 per cent inhibition (I50) of an enzymatic reaction. *Biochemical Pharmacology* 22:3099-3108.

20. Jorgensen WL, Chandrasekhar J, Madura JD, Impey RW, Klein ML (1983) Comparison of simple potential functions for simulating liquid water. *Journal of Chemical Physics* 79:926-935.

21. Pearlman DA, et al. (1995) AMBER, a package of computer programs for applying molecular mechanics, normal mode analysis, molecular dynamics and free energy calculations to simulate the structural and energetic properties of molecules. *Computer Physics Communications* 91:1-41.

22. Case D, et al. (2008) AMBER 10 (University of California, San Francisco).

23. Bayly C, Cieplak P, Cornell W, Kollman PA (1993) A well-behaved electrostatic potential based method using charge restraints for deriving atomic charges: the RESP model. *Journal of Physical Chemistry* 97:10269-10280.

24. Besler BH, Merz KM, Kollman PA (1990) Atomic charges derived from semiempirical methods. *Journal of Computational Chemistry* 11:431-439.

25. Singh UC, Kollman PA (2004) An approach to computing electrostatic charges for molecules. *Journal of Computational Chemistry* 5:129-145.

26. Frisch M, et al. (2004) Gaussian 03, Revision C.02 (Gaussian, Inc. , Wallingford, CT.).

27. Wang J, Cieplak P, Kollman P (2000) How well does a restrained electrostatic potential (RESP) model perform in calculating conformational energies of organic and biological molecules? *Journal of Computational Chemistry* 21:1049-1074.

28. Duke RE, Pedersen LG (2003) PMEMD 3 (University of North Carolina - Chapel Hill).

29. Darden T, York D, Pedersen L (1993) Particle mesh Ewald: An N*log(N) method for Ewald sums in large systems. *Journal of Chemical Physics* 98:10089-10092.

30. Röthlisberger D, et al. (2008) Kemp elimination catalysts by computational enzyme design. *Nature* 453:190-195.